

Learning Nonlinear Dynamics and Chaos: A Universal Framework for Knowledge-Based System Identification and Prediction

Tom Z. Jiahao¹, M. Ani Hsieh¹, and Eric Forgoston^{2*}
¹University of Pennsylvania, ²Montclair State University

We present a universal framework for learning the behavior of dynamical systems from observations. We formulate the learning task as a constrained optimization problem which can be efficiently solved using the adjoint sensitivity method. Our scheme is flexible with regards to the choice of model, and first-principles knowledge can be readily incorporated for hybrid learning. We demonstrate the effectiveness of our scheme by learning a variety of systems including a stiff Van der Pol oscillator, a chaotic Lorenz system, and the Kuramoto-Sivashinsky equation. We also include examples of hybrid learning and learning from noisy observations.

Data-driven system identification has a rich history in nonlinear dynamics and scientific machine learning. Various techniques have been developed to model and predict complex systems such as fluid dynamics and biological processes. One approach builds on Takens' embedding theorem and represents systems as time delay models by embedding the original system's states into delayed snapshots using an observation function [1]. Numerous modeling schemes including polynomial basis functions [2] and feedforward neural networks [3] were motivated by Takens' theorem and have been shown to work as effective time delayed models.

Modern machine learning strategies employ recurrent neural networks (RNNs), long-short term memory (LSTM), and reservoir computers (RCs). Different from feedforward neural networks, RNNs have memory properties as a result of a feedback loop. Both LSTMs [4] and RCs [5] are examples of RNNs that have been employed to predict two-dimensional fluid flows [6] and to describe the chaotic dynamics of a one-dimensional Kuramoto-Sivashinsky model [7]. Both time delay and RNN-based approaches model systems implicitly as they only provide outputs to the solutions of dynamical systems at prescribed time intervals. As such, the solutions lack continuity and thus it is difficult for the models to generalize across different initial conditions.

Recently, there has been an increased focus in developing strategies that learn the dynamics of a system by explicitly modeling its vector field rather than its solution. Existing methods include using sparse regression to determine the combination of basis functions that best describes the vector field from observations [8, 9]. A fundamental challenge with sparse regression is the need for a predetermined library of basis functions. If the correct terms are missing from the library, the resulting models may be inadequate at describing the system dynamics. As a result, bifurcations and chaotic behavior can be lost. In contrast, Chen *et al.* introduced a new family of neural networks, commonly referred to as neural ordinary differential equations (NODEs), which combines the power of modern machine learning with the formalism of differential equations to solve the data-driven

system identification problem [10]. NODEs formulate the identification task as an optimization problem and most commonly employ the adjoint sensitivity method for optimization [10–12]. NODEs using the adjoint sensitivity method have since been developed to improve model expressiveness [13], learn system dynamics from partial observations [14], and model the dynamics of stochastic processes [15]. Since the adjoint sensitivity method relies on the stability of the system to ensure the correct computation of gradients during optimization [16], existing NODE variants have yet to generalize to systems with unstable or chaotic dynamics.

In this letter we present a novel universal framework for learning the behavior of a general class of dynamical systems from observations. The learning task is formulated as a constrained optimization problem where the system dynamics are explicitly modeled as vector fields using neural networks. Leveraging the memory-efficiency of the adjoint sensitivity method, the proposed framework generalizes the learning task to any dynamical system including higher dimensional systems and those with unstable and chaotic behavior. In addition, we show how first principle knowledge can be readily incorporated for hybrid learning, significantly reducing the amount of data needed for training. In summary, the contribution of this work is a universal framework capable of: (1) modeling and prediction of systems with complex dynamics using neural networks; (2) bridging the gap between knowledge and true system dynamics through hybrid learning; and (3) leveraging inaccurately or inadequately identified models from sparse regression to recover true dynamics with lesser data.

Problem Formulation Given a dynamical system of the form $\dot{\mathbf{x}} = f(\mathbf{x}, t, \mathbf{p})$, where \mathbf{p} is the vector of parameters of the function f , and $\mathbf{x}(t) \in \mathbb{R}^n$ is the n -dimensional state vector at time t , we begin with the system identification problem. We are given m observations of the state from the trajectory or solution of f sampled at $T = \{t_1, t_2, \dots, t_m\}, t_i \in \mathbb{R}$. We denote these observations with the matrix $\mathbf{Z} \in \mathbb{R}^{m \times n}$. The i th row of \mathbf{Z} is the vector $\mathbf{z}(t_i) \in \mathbb{R}^n$, which is the observation of the state at t_i . Our goal is to approximate the function f with

$\hat{f}(\mathbf{x}, t, \boldsymbol{\theta})$ parameterized with the vector $\boldsymbol{\theta}$ based on the given observations \mathbf{Z} . In this work, we represent \hat{f} using an artificial neural network, though it can be represented using a linear combination of basis functions, or in the case of parameter estimation, can assume the form of f but with incorrect \mathbf{p} .

We then pose this system identification task as the following constrained optimization problem:

$$\begin{aligned} \min_{\boldsymbol{\theta}} \quad & L(\boldsymbol{\theta}) \\ \text{s.t.} \quad & \dot{\mathbf{x}} = \hat{f}(\mathbf{x}, t, \boldsymbol{\theta}), \quad \mathbf{x}(t_s, \mathbf{z}(t_s)) = \mathbf{z}(t_s), t_s \in T, \end{aligned} \quad (1)$$

where the first constraint is the differential equation defined by the vector field \hat{f} , the second constraint specifies the initial conditions, and the parameters $\boldsymbol{\theta}$ can then be estimated by $\boldsymbol{\theta} = \arg \min_{\boldsymbol{\theta}} L(\boldsymbol{\theta})$.

For the objective function in (1), we define an L^2 loss function between the observed trajectory and the trajectory generated by \hat{f} given by

$$L(\boldsymbol{\theta}) = \frac{1}{m - \alpha} \sum_{i=1}^{m-\alpha} \frac{1}{\alpha} \int_{t_i}^{t_i+\alpha} \delta(t_s - \tau) \|\mathbf{x}(\tau, \mathbf{z}(t_i)) - \mathbf{z}(\tau)\|^2 d\tau, \quad (2)$$

where $t_s \in T$ is any sampling time point, and δ is the Dirac delta function. In general, for any given initial condition, a trajectory can be generated from \hat{f} using a suitable numerical integration scheme. Thus, $\mathbf{x}(\tau, \mathbf{z}(t_i))$ in $L(\boldsymbol{\theta})$ is defined as the state at time τ generated by \hat{f} with the initial condition $\mathbf{x}(t_i, \mathbf{z}(t_i)) = \mathbf{z}(t_i)$ at time t_i given by

$$\mathbf{x}(\tau, \mathbf{z}(t_i)) = \mathbf{z}(t_i) + \int_{t_i}^{\tau} \hat{f}(\mathbf{x}(\omega, \mathbf{z}(t_i)), \omega, \boldsymbol{\theta}) d\omega. \quad (3)$$

Note that the state at t_{j+1} generated by \hat{f} with the initial condition $\mathbf{z}(t_j)$ is called a one-step-ahead diffeomorphic flow associated with \hat{f} . In our loss function given by (2), the integral from t_i to $t_i+\alpha$ requires an α -step-ahead diffeomorphism associated with \hat{f} , and we call α the *lookahead*. While some existing work assumes $\alpha = 1$ [8, 12, 17], we have found that using larger lookahead can sometimes yield better results. Hence we treat α as a hyperparameter to be tuned (see Supplemental Material S6).

Method To solve the optimization problem given by (1), we employ the adjoint sensitivity method [18] which gives the sensitivity of a model output with respect to its input. In our problem, the total derivative $d_{\boldsymbol{\theta}}L$ of the loss function with respect to the parameters $\boldsymbol{\theta}$ is the sensitivity we wish to evaluate. By defining an adjoint state, the sensitivity can be efficiently computed with constant memory cost by evaluating the adjoint state backwards along a given trajectory (see Supplemental Material S1 & S2). This is a marked contrast with the alternative of backpropagation, which requires one to

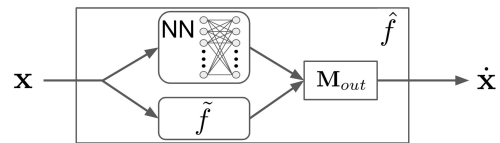


Figure 1: A hybrid architecture incorporating an imperfect vector field \tilde{f} into the model \hat{f} . Outputs from the neural network and the knowledge block \tilde{f} are then linearly coupled.

differentiate through numerical operations, saving all of the gradient information [10].

Knowledge In situations where partial knowledge of the dynamics exists, incorporating such knowledge can speed up the training process and improve model performance. Since our learning framework directly learns the vector field, there is high flexibility in the kind of knowledge that can be incorporated. In this letter, we will present a method to combine imperfect models with neural networks to improve model performance.

Given an imperfect model \tilde{f} as the knowledge, our neural network \hat{f} takes the form $\dot{\mathbf{x}}(t) = \hat{f}(\mathbf{x}, t, \tilde{f}(\mathbf{x}, t), \boldsymbol{\theta})$, where the output from \tilde{f} at any state is linearly coupled with \hat{f} using a matrix \mathbf{M}_{out} , which is co-trained with the neural network. The hybrid architecture is shown in Fig. 1. The ability to incorporate knowledge should require less training data for the learning framework to capture the true dynamics of the process of interest.

Results Using our universal learning framework, we consider different dynamical systems of varying complexities. For each system, training data is simulated with a suitable integration scheme. We validate the framework for learning the dynamics of systems without prior knowledge and with limited prior knowledge. The simulation and training parameters are summarized in Supplemental Material S4. Note that the training solver and its parameters must be chosen in a way such that it can realize the system's trajectories. For instance, Euler's method with a large step size may not suffice for stiff systems such as the Van der Pol oscillator as it will result in numerical instability. Selection of an appropriate training numerical solver can be achieved using existing physical insights into the system and available data.

The proposed framework is evaluated with respect to its ability to reproduce the dynamics of the actual system and to extrapolate or predict future observations. To determine if a system is chaotic, we perform the 0-1 test [19] on sufficiently long trajectories generated by that system. The test provides a diagnostic value K_c in which $K_c \approx 1$ for chaotic dynamics and $K_c \approx 0$ for regular dynamics (see Supplemental Material S3).

We first demonstrate our framework in learning the dynamics of a stiff system. Consider the *Van der Pol oscillator*, a non-conservative oscillator with a limit cycle behavior [20]. The oscillator's second-order differential

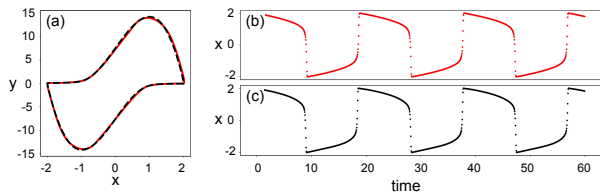


Figure 2: Prediction of the stiff Van der Pol oscillator with $\mu = 10$. (a) Simulated trajectory (red) versus the model predicted trajectory (dotted black). (b) True trajectory, and (c) predicted trajectory of x as a function of time for the Van der Pol oscillator.

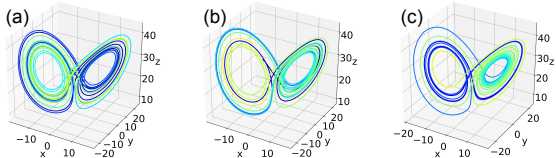


Figure 3: Learning the chaotic Lorenz system with a neural network without knowledge. (a) Training data ($t = 0$ to $t = 20$). (b) Model prediction ($t = 0$ to $t = 20$). (c) Model extrapolation ($t = 20$ to $t = 40$).

form is [21]

$$\frac{d^2x}{dt^2} = \mu(1 - x^2) \frac{dx}{dt} - x, \quad (4)$$

but it is often written in its first-order form as the system of equations $\dot{x} = y$; $\dot{y} = -x + \mu(y - x^2y)$. This system is known for its increasing *stiffness* as μ is increased. Here, we consider the stiff Van der Pol oscillator with $\mu = 10$. Training data is simulated with $\mu = 10$ and the initial condition $[x_0, y_0]^\top = [2, 0]^\top$. The trained model correctly captures the stiffness and limit cycle behavior of the Van der Pol oscillator as shown in Fig. 2.

Second, we consider the chaotic *Lorenz system* [22]

$$\begin{aligned} \dot{x} &= 10(y - x), & \dot{y} &= x(28 - z) - y, \\ \dot{z} &= xy - (8/3)z. \end{aligned} \quad (5)$$

We simulate training data with the initial condition $[x(0), y(0), z(0)]^\top = [-8, 7, 27]^\top$. As shown in Fig. 3, the trained model is able to capture the bistable structure of the Lorenz attractor both within and beyond the duration of the training data. Performing the 0-1 test on the predicted trajectory gives $K_c = 1.079$, showing that the identified system has chaotic dynamics.

Next, we consider the *Hopf normal form* [23],

$$\begin{aligned} \dot{x} &= \mu x + y - x(x^2 + y^2), \\ \dot{y} &= -x + \mu y - y(x^2 + y^2), \end{aligned} \quad (6)$$

where μ is the system parameter which, when varied, gives rise to a Hopf bifurcation. We incorporate the parameter μ into our model as a third dimension to the input vector, and set its time derivative to 0, i.e. $\dot{\mu} = 0$.

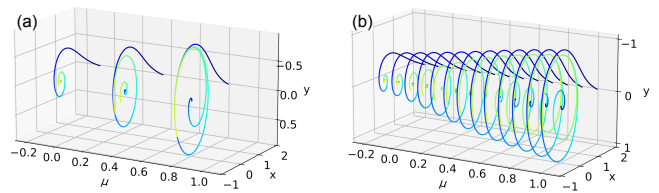


Figure 4: Learning the Hopf normal form. (a) Training data. (b) The trained model interpolates between $\mu = -0.2$ to $\mu = 1.0$.

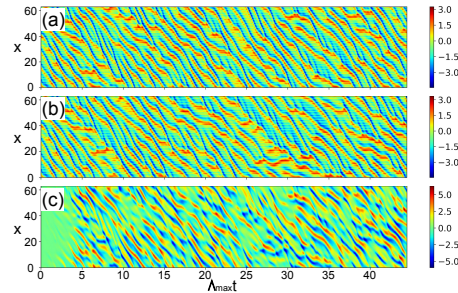


Figure 5: Trained KS model prediction on the testing data. (a) Testing data. (b) Prediction with the trained model using the first step of test data as the initial condition. (c) Difference between the test data and prediction.

Training data, as shown in Fig. 4(a), is simulated with three parameter values $\mu = \{-0.1, 0.35, 0.8\}$. The trained model correctly captures the bifurcation as shown in Fig. 4(b). The trained model can accurately interpolate between $\mu = -0.1$ to $\mu = 0.8$, and extrapolate from $\mu = -0.2$ to $\mu = 1.0$, which is beyond the range of μ in the training data.

Moreover, our framework can learn the dynamics of spatiotemporally chaotic PDEs. Consider the one-dimensional *Kuramoto-Sivashinsky equation* (KS) with periodic boundary conditions $y = y(x, t)$ and $y(x + L, t) = y(x, t)$ [24, 25]

$$\frac{\partial y}{\partial t} = -y \frac{\partial y}{\partial x} - \frac{\partial^2 y}{\partial x^2} - \frac{\partial^4 y}{\partial x^4}. \quad (7)$$

We consider a 64-grid KS equation with $L = 60$. The most positive Lyapunov exponent is $\Lambda_{max} = 0.089$, and the Kaplan-Yorke dimension of the attractor is $D_{KY} = 13.56$ [26]. We use a natural time scale, the Lyapunov time $\Lambda_{max}t$, for model evaluation. Since this system is spatially high-dimensional, we use convolutional layers in our neural network to reduce both its dimensionality and the number of parameters in the model. Fig. 5 shows that the trained neural network can capture the first 4 Lyapunov times with high accuracy before the trajectories diverge. Even after the trajectories diverge, the system behaves similarly to the actual system.

It is also possible to perform *knowledge-based learning* with our framework. First we consider a Lorenz system with modified coefficients from (5). The modified system

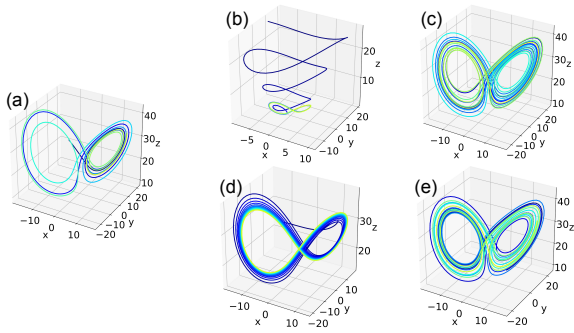


Figure 6: Learning the Lorenz system with knowledge. (a) Training data ($t = 0$ to $t = 8$). (b) Trajectory ($t = 0$ to $t = 20$) of the modified Lorenz system, which has periodic rather than chaotic behavior. We combine this modified system with a neural network according to the hybrid scheme shown in Fig. 1. The training data, shown in Fig. 6(a), is generated with the initial condition $[x(0), y(0), z(0)]^T = [-8, 7, 27]^T$. Note that this training data has only $2/5$ the length used for training without knowledge. Fig. 6(c) shows that the trained model restores the bistable structure and chaotic dynamics. Performing the 0-1 test on the knowledge gives $K_c = 0.036$, and the predicted trajectory gives $K_c = 1.11$, showing that the trained model has chaotic dynamics.

keeps \dot{x} and \dot{z} the same but has $\dot{y} = x(-4.7 - z) + 7.2y$. Fig. 6(b) shows the trajectory of this modified system, which has periodic rather than chaotic behavior. We combine this modified system with a neural network according to the hybrid scheme shown in Fig. 1. The training data, shown in Fig. 6(a), is generated with the initial condition $[x(0), y(0), z(0)]^T = [-8, 7, 27]^T$. Note that this training data has only $2/5$ the length used for training without knowledge. Fig. 6(c) shows that the trained model restores the bistable structure and chaotic dynamics. Performing the 0-1 test on the knowledge gives $K_c = 0.036$, and the predicted trajectory gives $K_c = 1.11$, showing that the trained model has chaotic dynamics.

Next, we use a SINDy-identified system as knowledge. SINDy is a system identification method which performs sparse regression on a library of functions [8]. When xy and xz are excluded from the library of functions, SINDy incorrectly identifies $\dot{y} = -7.175x + 20.507y - 0.613yz$, and $\dot{z} = -3.05z + 0.504x^2 + 0.479y^2$. Both \dot{y} and \dot{z} have incorrect nonlinearities. Fig. 6(d) shows the trajectory of this incorrectly identified system, which has periodic behavior. The trained model can correctly extrapolate to capture the bistable structure as shown in Fig. 6(e). Performing the 0-1 test on the knowledge gives $K_c = 0.064$, and the predicted trajectory gives $K_c = 0.832$, showing that the trained model has chaotic dynamics.

We used our framework with the same amount of data without knowledge. The neural network tends to “memorize” the data and gives low training error. However when further extrapolating in time, the trained model tends to either a limit cycle or fixed point.

Lastly, we demonstrate our framework’s robustness to observational noise. Considering the Lorenz system, we use the same training data as training without knowledge but now include Gaussian noise with zero mean and 0.1 variance ($\sim N(0, 0.1)$). This noisy trajectory is shown in

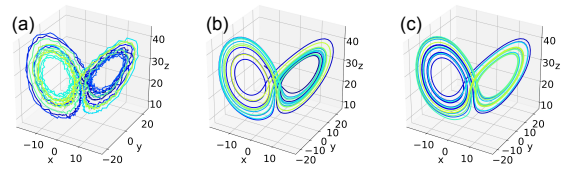


Figure 7: Learning the Lorenz system from noisy observations. (a) Training data ($t = 0$ to $t = 20$) with observational noise $\sim N(0, 0.1)$. (b) Model prediction ($t = 0$ to $t = 20$). (c) Model extrapolation ($t = 20$ to $t = 40$).

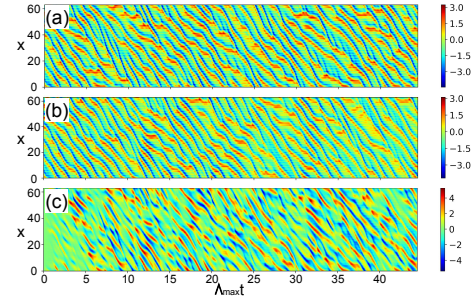


Figure 8: Learning from noisy observations of KS equation. (a) Testing data with $\sim N(0, 0.01)$ Gaussian noise. (b) Prediction with the trained model using the first step of test data as the initial condition. (c) Difference between the test data and prediction

Fig. 7(a). The trained neural network correctly captures the bistable structure for both within and beyond the duration of the training data, as shown in Fig. 7(b) and 7(c). Performing the 0-1 test on the predicted trajectory gives $K_c = 1.10$, showing that the trained neural network possesses chaotic dynamics.

The same neural network architecture converges much faster when trained on noisy observations of the Lorenz system. With the Adam optimizer, the result in Fig. 7 takes 500 epochs to train on noisy observations, while the result in Fig. 3 takes more than 3000 training epochs. These observations are consistent with recent work that adds noise to observations of chaotic systems to stabilize the training process [7].

We also consider noisy observations from the KS equation. Using the same training data as learning without knowledge, we include Gaussian noise with zero mean and 0.01 variance ($\sim N(0, 0.01)$). Fig. 8 shows the learning result. Though the trained model can only accurately predict about 1 Lyapunov time before the trajectories diverge, this demonstrates the effect of noise on the chaotic dynamics, *i.e.* a slight perturbation in the initial condition as a result of noise makes the trajectories diverge exponentially fast. However, it can be seen that the predicted trajectories behave similarly to the true system.

Discussion and Conclusion We have demonstrated the universality of our framework by learning a wide variety of systems including stiff, bifurcating, and chaotic systems. We have also shown that with spatial convolution, our

framework can easily scale and model high-dimensional systems. Note that since our framework does not require fixed time intervals for the training data, it can also learn from irregularly sampled trajectories.

In this framework, the neural network is trained with respect to a numerical solver which can be different from the simulation solver used to generate the training data. In our work, KS training data was generated using an ET-DRK4 method, but the neural network was trained using Euler’s method. This means that we have the freedom to choose the training solver and its parameters depending on our needs. For example, we can use lower order solvers to speed up training at the expense of model accuracy, and we can perform finer temporal interpolations by using a smaller step size for the training solver at the expense of training speed. This is an important feature that ensures excellent accuracy without sacrificing computational speed. Moreover, it ensures that our framework can be applied not only in the case when one has high-fidelity simulation data, but also when one is working with real data, that may be noisy or have missing/sparse data.

For future work, we seek to explore more hybrid-learning approaches by incorporating different types of knowledge. We also hope to study stochastic dynamics by extending this work to stochastic differential equations. Moreover, besides using spatial convolutions for dimension reduction, we will investigate parallel learning using our framework to achieve even better scalability for very high-dimensional systems. In addition, we plan to use the framework to extract additional physical insight into a wide range of dynamical systems. Given the amount of model and real data available to us, and considering the complexity of these systems, our universal learning framework can be used to understand meaningful correlations and establish new relationships between processes, thereby enhancing our knowledge.

Acknowledgement This work was funded by the Office of Naval Research (ONR) Award No. 14-19-1-2253.

* {zjh,m.hsieh}@seas.upenn.edu,
eric.forgoston@montclair.edu

- [1] F. Takens, Detecting strange attractors in turbulence, in *Dynamical systems and turbulence*, edited by D. A. Rand and L. S. Young (Springer-Verlag, New York, 1980) pp. 366–381.
- [2] J. Paduart, L. Lauwers, J. Swevers, K. Smolders, J. Schoukens, and R. Pintelon, Identification of nonlinear systems using polynomial nonlinear state space models, *Automatica* **46**, 647 (2010).
- [3] E. Wan, Time series prediction by using a connectionist network with internal delay lines, *Time Series Prediction by Using a Connectionist Network with Internal Delay Lines* (2000).
- [4] S. Hochreiter and J. Schmidhuber, Long short-term memory, *Neural computation* **9**, 1735 (1997).
- [5] H. Jaeger, The ‘echo state’ approach to analysing and training recurrent neural networks-with an erratum note’, Bonn, Germany: German National Research Center for Information Technology GMD Technical Report **148** (2001).
- [6] M. Qraitem, D. Kularatne, E. Forgoston, and M. A. Hsieh, Bridging the gap: Machine learning to resolve improperly modeled dynamics, *Physica D: Nonlinear Phenomena* **414**, 10.1016/j.physd.2020.132736 (2020).
- [7] A. Wikner, J. Pathak, B. Hunt, M. Girvan, T. Arcomano, I. Szunyogh, A. Pomerance, and E. Ott, Combining machine learning with knowledge-based modeling for scalable forecasting and subgrid-scale closure of large, complex, spatiotemporal systems, *Chaos: An Interdisciplinary Journal of Nonlinear Science* **30**, 053111 (2020).
- [8] S. Brunton, J. Proctor, and J. Kutz, Discovering governing equations from data: Sparse identification of nonlinear dynamical systems, *Proceedings of the National Academy of Sciences* **113**, 3932–3937 (2015).
- [9] A. A. AlMomani, J. Sun, and E. Bollt, How entropic regression beats the outliers problem in nonlinear system identification, *Chaos* **30**, 013107 (2020).
- [10] T. Q. Chen, Y. Rubanova, J. Bettencourt, and D. Duvenaud, Neural ordinary differential equations., in *NeurIPS*, edited by S. Bengio, H. M. Wallach, H. Larochelle, K. Grauman, N. Cesa-Bianchi, and R. Garnett (2018) pp. 6572–6583.
- [11] C. Zang, P. Cui, W. Zhu, and F. Wang, Dynamical origins of distribution functions, *Proceedings of the 25th ACM SIGKDD International Conference on Knowledge Discovery & Data Mining* 10.1145/3292500.3330842 (2019).
- [12] S. Ouala, D. Nguyen, L. Drumetz, B. Chapron, A. Pascual, F. Collard, L. Gaultier, and R. Fablet, Learning latent dynamics for partially-observed chaotic systems (2019), [arXiv:1907.02452 \[stat.ML\]](https://arxiv.org/abs/1907.02452).
- [13] E. Dupont, A. Doucet, and Y. W. Teh, Augmented neural odes, in *Advances in Neural Information Processing Systems 32* (Curran Associates, Inc., 2019) pp. 3140–3150.
- [14] I. Ayed, E. de Bézenac, A. Pajot, J. Brajard, and P. Gallinari, Learning dynamical systems from partial observations., *CoRR abs/1902.11136* (2019).
- [15] X. Li, T.-K. L. Wong, R. T. Q. Chen, and D. Duvenaud, Scalable gradients for stochastic differential equations (PMLR, Online, 2020) pp. 3870–3882.
- [16] I. M. Ross., A primer on pontryagin’s principle in optimal control (Collegiate publishers San Francisco, 2009).
- [17] M. Raissi, P. Perdikaris, and G. Karniadakis, Multistep neural networks for data-driven discovery of nonlinear dynamical systems, *arXiv: Dynamical Systems* (2018).
- [18] Y. Cao, S. Li, L. Petzold, and R. Serban, Adjoint sensitivity analysis for differential-algebraic equations: The adjoint dae system and its numerical solution, *SIAM J. Sci. Comput.* **24**, 1076 (2003).
- [19] G. Gottwald and I. Melbourne, A new test for chaos in deterministic systems, *Proceedings of the Royal Society of London, Series A: Mathematical, Physical and Engineering Sciences* **460**, 603–611 (2004).
- [20] R. H. Enns and G. McGuire, Limit cycles, in *Nonlinear Physics with Maple for Scientists and Engineers* (Birkhäuser Boston, Boston, MA, 1997) pp. 183–208.
- [21] B. van der Pol Jun. D.Sc, Lxxxviii. on “relaxation-oscillations”, *The London, Edinburgh, and Dublin Philosophical Magazine and Journal of Science* **2**, 978 (1926).
- [22] E. N. Lorenz, Deterministic nonperiodic flow, *Journal of the Atmospheric Sciences* **20**, 130 (1963).

- [23] M. M. J. E. Marsden, *The Hopf Bifurcation and Its Applications* (Springer-Verlag New York, 1976).
- [24] Y. Kuramoto, Diffusion-induced chaos in reaction systems, *Progress of Theoretical Physics Supplement* **64**, 346 (1978), <https://academic.oup.com/ptps/article-pdf/doi/10.1143/PTPS.64.346/5293041/64-346.pdf>.
- [25] G. Sivashinsky, Nonlinear analysis of hydrodynamic instability in laminar flames—i. derivation of basic equations, *Acta Astronautica* **4**, 1177 (1977).
- [26] R. A. EDSON, J. E. BUNDER, T. W. MATTNER, and A. J. ROBERTS, Lyapunov exponents of the kuramoto–sivashinsky pde, *The ANZIAM Journal* **61**, 270–285 (2019).
- [27] M. Surtsukov, neural-ode, <https://github.com/msurtsukov/neural-ode> (2019).
- [28] H. D. I. Abarbanel, R. Brown, J. J. Sidorowich, and L. S. Tsimring, The analysis of observed chaotic data in physical systems, *Rev. Mod. Phys.* **65**, 1331 (1993).
- [29] J. P. Eckmann, S. O. Kamphorst, D. Ruelle, and S. Ciliberto, Liapunov exponents from time series, *Phys. Rev. A* **34**, 4971 (1986).
- [30] K. Sun, X. Liu, and C.-X. Zhu, The 0-1 test algorithm for chaos and its applications, *Chinese Physics B - CHIN PHYS B* **19** (2010).
- [31] S. Cox and P. Matthews, Exponential time differencing for stiff systems, *Journal of Computational Physics* **176**, 430 (2002).

SUPPLEMENTAL MATERIAL

S1: Adjoint Sensitivity Method

Given the loss function

$$L(\boldsymbol{\theta}) = \frac{1}{m-\alpha} \sum_{i=1}^{m-\alpha} \frac{1}{\alpha} \int_{t_i}^{t_{i+\alpha}} \delta(t_s - \tau) \|\mathbf{x}(\tau, \mathbf{z}(t_i)) - \mathbf{z}(\tau)\|^2 d\tau, \quad (8)$$

and the optimization problem

$$\begin{aligned} \min_{\boldsymbol{\theta}} \quad & L(\boldsymbol{\theta}) \\ \text{s.t.} \quad & \dot{\mathbf{x}} = \hat{f}(\mathbf{x}, t, \boldsymbol{\theta}), \\ & \mathbf{x}(t_s, \mathbf{z}(t_s)) = \mathbf{z}(t_s), t_s \in T, \end{aligned} \quad (9)$$

we consider the subproblem of minimizing the integral $\int_{t_i}^{t_{i+\alpha}} \delta(t_s - \tau) \|\mathbf{x}(\tau, \mathbf{z}(t_i)) - \mathbf{z}(\tau)\|^2 d\tau$. The full optimization problem is then the sum of $m - \alpha$ subproblems. The subproblem is given by

$$\begin{aligned} \min_{\boldsymbol{\theta}} \quad & F(\boldsymbol{\theta}) = \int_{t_i}^{t_{i+\alpha}} \delta(t_s - \tau) \|\mathbf{x}(\tau, \mathbf{z}(t_i)) - \mathbf{z}(\tau)\|^2 d\tau \\ \text{s.t.} \quad & h(\mathbf{x}, \dot{\mathbf{x}}, \boldsymbol{\theta}, t) = 0 \\ & g(\mathbf{x}(t_i), \mathbf{z}(t_i)) = 0, \end{aligned} \quad (10)$$

where the first constraint is the implicit form of $\dot{\mathbf{x}} = \hat{f}(\mathbf{x}, t, \boldsymbol{\theta})$ given by $h(\mathbf{x}, \dot{\mathbf{x}}, \boldsymbol{\theta}, t) = \dot{\mathbf{x}} - \hat{f}(\mathbf{x}, t, \boldsymbol{\theta}) = 0$. The second constraint specifies the initial conditions used for the integral where $\mathbf{x}(t_i, \mathbf{z}(t_i)) = \mathbf{z}(t_i)$ and thus $g(\mathbf{x}(t_i), \mathbf{z}(t_i)) = \mathbf{x}(t_i, \mathbf{z}(t_i)) - \mathbf{z}(t_i) = 0$.

The optimization algorithm is based on the adjoint sensitivity method [18], and the full derivation can be found in the next section. First we numerically solve $\dot{\mathbf{x}} = \hat{f}(\mathbf{x}, t, \boldsymbol{\theta})$ for its trajectory forward in time from t_i to $t_{i+\alpha}$ with the specified initial conditions. Then we define the adjoint equation as:

$$2\delta(t_s - t)(\mathbf{x}(t) - \mathbf{z}(t)) - \boldsymbol{\lambda}^\top \hat{f}_{\mathbf{x}} - \dot{\boldsymbol{\lambda}}^\top = 0, \quad (11)$$

where $\boldsymbol{\lambda}$ is a continuous-time Lagrange multiplier except at the sampling times. We then numerically solve this equation backwards in time with the initial conditions $\boldsymbol{\lambda}(t_{i+\alpha}) = 0$ to obtain the trajectory of $\boldsymbol{\lambda}$ from $t = i + \alpha$ to $t = i$. Lastly the gradient of F with respect to the parameters $\boldsymbol{\theta}$ is given by its total derivative

$$d_{\boldsymbol{\theta}} F = - \int_{t_i}^{t_j} \boldsymbol{\lambda}^\top \hat{f}_{\boldsymbol{\theta}} dt. \quad (12)$$

After obtaining the gradient, we can then perform optimization with methods such as stochastic gradient descent. Note that the Jacobians $\hat{f}_{\mathbf{x}}$ and $\hat{f}_{\boldsymbol{\theta}}$ can be computed efficiently with automatic differentiation during the forward pass. In summary, the optimization algorithm involves the following steps:

1. Numerically solve $\dot{\mathbf{x}} = \hat{f}(\mathbf{x}, t, \boldsymbol{\theta})$ forward in time from t_i to $t_{i+\alpha}$.
2. Numerically solve the adjoint equation (11) backward in time from $t_{i+\alpha}$ to t_i using the initial conditions $\boldsymbol{\lambda}(t_{i+\alpha}) = 0$.
3. Evaluate the integral (12) to obtain the desired gradient.

For the PyTorch implementation of this optimization algorithm, we referenced [27].

S2: Adjoint Sensitivity Method Derivation

Consider the following optimization problem

$$\begin{aligned} \min_{\boldsymbol{\theta}} \quad & F(\boldsymbol{\theta}) = \int_{t_i}^{t_j} D(\mathbf{x}(t), t) dt \\ \text{s.t.} \quad & h(\mathbf{x}, \dot{\mathbf{x}}, \boldsymbol{\theta}, t) = 0 \\ & g(\mathbf{x}(t_i), t_i) = 0, \end{aligned} \quad (13)$$

where $h(\mathbf{x}, \dot{\mathbf{x}}, t, \boldsymbol{\theta}) = \dot{\mathbf{x}} - \hat{f}(\mathbf{x}, \boldsymbol{\theta}, t) = 0$ and $g(\mathbf{x}(t_i), t_i) = \mathbf{x}(t_i) - \mathbf{z}(t_i) = 0$.

Introducing the Lagrangian, we have

$$\mathcal{L} = \int_{t_i}^{t_j} D(\mathbf{x}(t), t) + \boldsymbol{\lambda}^\top h(\mathbf{x}, \dot{\mathbf{x}}, \boldsymbol{\theta}, t) dt + \boldsymbol{\mu}^\top g(\mathbf{x}(t_i), t_i), \quad (14)$$

where $\boldsymbol{\lambda}$ and $\boldsymbol{\mu}$ are Lagrange multipliers and $\boldsymbol{\lambda}$ is time-varying. The total derivative of \mathcal{L} with respect to $\boldsymbol{\theta}$ is

$$\begin{aligned} d_{\boldsymbol{\theta}} \mathcal{L} = \int_{t_i}^{t_j} D_{\mathbf{x}} d_{\boldsymbol{\theta}} \mathbf{x} + D_{\boldsymbol{\theta}} + \boldsymbol{\lambda}^\top (h_{\dot{\mathbf{x}}} d_{\boldsymbol{\theta}} \dot{\mathbf{x}} + h_{\mathbf{x}} d_{\boldsymbol{\theta}} \mathbf{x} + h_{\boldsymbol{\theta}}) dt \\ + \boldsymbol{\mu}^\top (g_{\mathbf{x}} d_{\boldsymbol{\theta}} \mathbf{x}|_{t_i} + g_{\boldsymbol{\theta}}). \end{aligned} \quad (15)$$

Consider the term $\boldsymbol{\lambda}^\top h_{\dot{\mathbf{x}}} d_{\boldsymbol{\theta}} \dot{\mathbf{x}}$ in the integrand. Using integration by parts, we have

$$\begin{aligned} \int_{t_i}^{t_j} \boldsymbol{\lambda}^\top h_{\dot{\mathbf{x}}} d_{\boldsymbol{\theta}} \dot{\mathbf{x}} dt = \boldsymbol{\lambda}^\top h_{\dot{\mathbf{x}}} d_{\boldsymbol{\theta}} \mathbf{x}|_{t_i}^{t_j} - \\ \int_{t_i}^{t_j} \left(\dot{\boldsymbol{\lambda}}^\top h_{\dot{\mathbf{x}}} + \boldsymbol{\lambda}^\top d_t h_{\dot{\mathbf{x}}} \right) d_{\boldsymbol{\theta}} \mathbf{x} dt. \end{aligned} \quad (16)$$

Substituting (16) into (15), the Lagrangian becomes

$$\begin{aligned} d_{\boldsymbol{\theta}} \mathcal{L} = \int_{t_i}^{t_j} \left(D_{\mathbf{x}} + \boldsymbol{\lambda}^\top (h_{\mathbf{x}} - d_t h_{\dot{\mathbf{x}}}) - \dot{\boldsymbol{\lambda}}^\top h_{\dot{\mathbf{x}}} \right) d_{\boldsymbol{\theta}} \mathbf{x} + D_{\boldsymbol{\theta}} + \\ \boldsymbol{\lambda}^\top h_{\boldsymbol{\theta}} dt + \boldsymbol{\lambda}^\top h_{\dot{\mathbf{x}}} d_{\boldsymbol{\theta}} \mathbf{x}|_{t_i}^{t_j} + \boldsymbol{\mu}^\top (g_{\mathbf{x}} d_{\boldsymbol{\theta}} \mathbf{x}|_{t_i} + g_{\boldsymbol{\theta}}). \end{aligned}$$

The last term is 0 since at t_i , \mathbf{x} does not depend on $\boldsymbol{\theta}$, and g does not depend on \mathbf{x} or $\boldsymbol{\theta}$. Also $h_{\dot{\mathbf{x}}} = I$ and its time derivative $d_t h_{\dot{\mathbf{x}}}$ is 0. D does not directly depend on $\boldsymbol{\theta}$ so $D_{\boldsymbol{\theta}}$ is also 0. For our problem, this expression finally simplifies to

$$d_{\boldsymbol{\theta}} \mathcal{L} = \int_{t_i}^{t_j} \left(D_{\mathbf{x}} + \boldsymbol{\lambda}^\top h_{\mathbf{x}} - \dot{\boldsymbol{\lambda}}^\top \right) d_{\boldsymbol{\theta}} \mathbf{x} + \boldsymbol{\lambda}^\top h_{\boldsymbol{\theta}} dt + \boldsymbol{\lambda}^\top d_{\boldsymbol{\theta}} \mathbf{x}|_{t_j}. \quad (17)$$

To avoid computing $d_{\theta}\mathbf{x}$ inside the integral, one can set the term in parentheses to zero, thereby giving the adjoint equation

$$D_{\mathbf{x}} + \boldsymbol{\lambda}^{\top} h_{\mathbf{x}} - \dot{\boldsymbol{\lambda}}^{\top} = 0. \quad (18)$$

One can avoid computing $d_{\theta}\mathbf{x}$ at t_j in (17) by setting $\boldsymbol{\lambda}^{\top}(t_j) = 0$. This is appropriate as long as the system under consideration is an index-0 or index-1 DAE system [18].

Lastly the total derivative of F with respect to the parameter θ is

$$d_{\theta}F = \int_{t_i}^{t_j} \boldsymbol{\lambda}^{\top} h_{\theta} dt.$$

Since $h_{\theta} = -\hat{f}_{\theta}$, the expression can be rewritten as

$$d_{\theta}F = - \int_{t_i}^{t_j} \boldsymbol{\lambda}^{\top} \hat{f}_{\theta} dt. \quad (19)$$

S3: Determining Chaos

To determine whether a system is truly chaotic, we employ the 0-1 test proposed by Gottwald and Melbourne [19]. Different from computing Lyapunov exponents [28, 29], the 0-1 test directly applies to time series data and does not require phase space reconstruction. Additionally this test is binary, *i.e.*, it outputs 1 if the system is chaotic and 0 otherwise, under ideal conditions. We briefly summarize the methodology and refer the interested reader to [30] for the implementation details.

Consider a one-dimensional time series with data $z(t_n)$ for $n = 1, 2, \dots, N$ such that the data is used to drive the two-dimensional system given by

$$\begin{aligned} p_c(n+1) &= p_c(n) + z(t_n) \cos(nc), \\ q_c(n+1) &= q_c(n) + z(t_n) \sin(nc), \end{aligned} \quad (20)$$

where $c \in (0, \pi)$ is a hyperparameter. For systems with regular dynamics, p_c and q_c are bounded, while for chaotic dynamics, they approximately follow Brownian motion with zero drift [19]. Figure 9 shows trajectories of p_c and q_c for the Lorenz systems exhibiting regular and chaotic dynamics.

Let the mean square displacement for $n = 1, 2, 3, \dots$ be given by

$$M_c(n) = \lim_{N \rightarrow \infty} \frac{1}{N} \sum_{i=1}^N ([p_c(i+n) - p_c(i)]^2 + [q_c(i+n) - q_c(i)]^2).$$

The asymptotic growth rate of this system is then

$$K_c = \lim_{n \rightarrow \infty} \frac{\log M_c(n)}{\log n}.$$

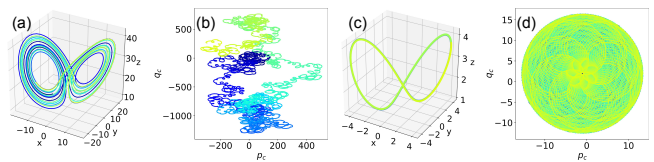


Figure 9: Performing the 0-1 test on the chaotic and non-chaotic Lorenz system. We use $N = 10000$ and $c = 0.4$, with trajectories sampled with a time interval of 0.05. (a) Trajectories of a chaotic Lorenz system. (b) Unbounded p_c and q_c for the chaotic Lorenz system, with $K_c = 1.12$. (c) Trajectories of a non-chaotic Lorenz system. (d) Bounded p_c and q_c for the non-chaotic Lorenz system, with $K_c = 0.036$.

such that systems with chaotic dynamics result in $K_c = 1$ and those with regular dynamics result in $K_c = 0$. In practice, observational data streams are finite and thus the asymptotic growth rate is approximated using the slope of $\log M_c(n)$. Thus, when data streams are finite, $K_c \approx 1$ and $K_c \approx 0$ for chaotic and regular dynamics respectively. For continuous-time systems, the trajectories must be sampled with equal and sufficiently coarse intervals for good results. For systems with dimension greater than one, each dimension is tested separately and if $K_c \approx 1$ for any single dimension, then the test implies the presence of chaotic dynamics.

In this work, for all the 0-1 tests that were performed, we first simulated 55000 data points and discarded the first 5000 transient data points so that the tested trajectory lies on the attractor. Then we sample the trajectory with a sampling step size of 0.05, which provides $N = 10000$ data points. We finally perform the 0-1 test on this sampled trajectory with $c = 0.4$. Note that though theoretically any values of $c \in (0, \pi)$ should work, it is possible for a chaotic system to be tested as non-chaotic for some values of c . Therefore, a more accurate approach is to perform the 0-1 test with a range of values of c , with the diagnostic output computed as an average.

S4: Simulation and Training Parameters

In this section, we summarize for each system the solvers and parameters used for data simulation and neural network training. For each system under consideration, a suitable numerical integration scheme is used to simulate observations. For example, a variable-order, variable-step ODE solver is used to simulate the stiff Van der Pol equation while the fourth-order Runge-Kutta scheme (RK4) generally suffices for non-stiff systems. We call this solver the simulation solver. Since we train neural networks to represent vector fields, trajectories must also be realized through a numerical integration scheme, which we call the training solver. The simulation and training solvers and parameters are summarized in Table I.

The simulation solver and the training solver do not nec-

System	Simulation Solver	Δt_{sim}	T_{sim}	Δt_{sam}	Training Solver	Lookahead
1	SciPy vode (order =15)	0.05	50	0.05	SciPy vode (order =15)	1
2	ETDRK4	0.25	1250	0.25	Euler's Method	2
3	RK4	0.01	10	0.02	RK4	2
4	RK4	0.01	20	0.02	RK4	2
5	RK4	0.01	8	0.02	RK4	2
6	RK4	0.01	8	0.02	RK4	2
7	RK4	0.01	20	0.02	RK4	2

Table I: Simulation and training parameters of all systems. Δt_{sim} is the simulation time step; T_{sim} is the simulation duration; Δt_{sam} is the sampling time step. The systems are 1. Van der Pol oscillator 2. KS equation 3. Hopf normal form 4. Lorenz system (learning without knowledge) 5. Lorenz system (learning with a modified system as knowledge) 6. Lorenz system (learning with a SINDy-identified system as knowledge) 7. Lorenz system (noisy observations).

Layer	# of Hidden Units	Activation
1	256	ReLU

Table II: Neural network architecture for learning the Hopf normal form, Lorenz system without knowledge, and noisy Lorenz system.

essarily need to be same, as demonstrated by our results for learning the KS equation. Data is simulated for the KS equation using the fourth-order Runge-Kutta exponential time differencing (ETDRK4) integration scheme [31]. We discard the first 1000 steps of transient data and simulate a total of 8000 steps. Training data is taken to be the first 5000 steps, which equates to 111.25 Lyapunov time. Testing data is taken from the 6000th to the 8000th steps of the simulated data.

The neural network architectures used for learning the systems are summarized in Table II, III, IV, and V. Note that for learning with knowledge, the output (dimension = 3) from the neural network (Table III) is linearly coupled with the output from the knowledge component with a matrix \mathbf{M}_{out} , which is co-trained with the neural network. Moreover for learning the KS equation, the output (dimension = 2048) from the convolutional layers (Table V) is restored to the original spatial size (dimension = 64) with a linear coupling matrix, which is also co-trained with the neural network.

Through experiments, we note that the *tanh* activation

Layer	# of Hidden Units	Activation
1	32	ReLU
2	512	ReLU
3	32	ReLU

Table III: Neural network architecture for learning with knowledge (for both learning with a non-chaotic Lorenz system and with a SINDy-identified incorrect system).

Layer	# of Hidden Units	Activation
1	512	Tanh
2	32	Softplus($\beta = 1.8$)

Table IV: Neural network architecture for learning the Van der Pol oscillator.

Layer	Type	Channel Out	Kernel Size	Stride	Padding	Activation
1	Conv	32	3	1	1	Leaky ReLU
2	Conv	256	3	1	1	Leaky ReLU
3	Conv	128	3	1	1	Tanh
4	Conv	128	3	1	1	Leaky ReLU
5	Conv	128	3	2	1	Leaky ReLU
6	Conv	128	3	2	1	None

Table V: Neural network architecture for learning the KS equation.

function tends to encourage periodicity in the solutions, and *Leaky ReLU* works better than *ReLU* for producing high-dimensional chaos. Through the Van der Pol oscillator example, we have also shown that *Softplus*, a smooth approximation of *ReLU* is also an effective activation function for learning dynamics.

S5: Comments on SINDy

As we have mentioned, system identification methods that use sparse regression on library of basis functions face the fundamental challenge of choosing the correct terms. In this section we will consider one of these methods, Sparse Identification of Nonlinear Dynamics (SINDy) [8], and demonstrate how it can incorrectly identify a nonlinear system.

To perform SINDy, We simulate the chaotic Lorenz system using RK4 with a step size of 0.01 from $t = 0$ to $t = 80$ and sample training data with a step size of 0.02. We then perform SINDy on this data using a library of polynomials up to the fourth order. If we include the

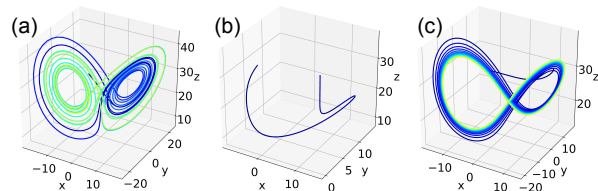


Figure 10: Systems identified by SINDy using a library of polynomial functions up to the fourth order after excluding different nonlinearities from the function library. Each plot shows the a trajectory for $t = 0$ to $t = 20$. (a) System identified if all terms are included in the library. (b) System identified if x , xy , and xz are excluded from the library. (c) System identified if xy and xz are excluded from the library.

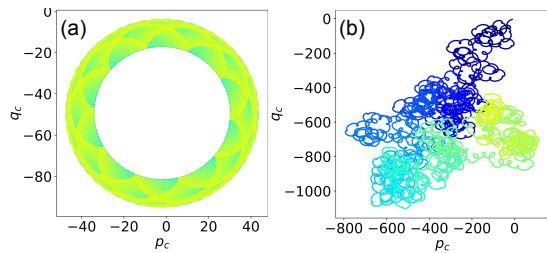


Figure 11: Plots of q_c against p_c for the incorrectly identified system by SINDy and the trained model using the proposed framework. (a) Bounded q_c and p_c for the incorrectly identified system by SINDy when xy and xz are excluded from the library of functions. $K_c = 0.064$. (b) Unbounded q_c and p_c for the trained model using the proposed framework. $K_c = 0.832$.

correct functions, i.e. x, y, z, xy , and xz in the library, SINDy will identify the system as

$$\begin{aligned}\dot{x} &= -9.913x + 9.913y, \\ \dot{y} &= 27.212x - 0.848y - 0.978xz, \\ \dot{z} &= 0.988xy - 2.636z.\end{aligned}\quad (21)$$

This identified system, as shown in Fig. 10(a), is a very close representation of the true system. Its form in (21) only has slightly different coefficients from the actual system. However if the nonlinearities xz and xy are excluded from the library of functions, SINDy identifies a system shown in Fig. 10(c). This system is not chaotic as the trajectory eventually forms a "8"-shaped limit cycle. This system has the form

$$\begin{aligned}\dot{x} &= -9.913x + 9.913y, \\ \dot{y} &= -7.175x + 20.507y - 0.613yz, \\ \dot{z} &= -3.05z + 0.504x^2 + 0.479y^2.\end{aligned}\quad (22)$$

It can be seen that \dot{y} and \dot{z} do not have the correct nonlinearities. If x, xz , and xy are excluded, the identified system, as shown in Fig. 10(b), fails completely to capture the bistable structure.

In this work, we have shown that our framework is able to leverage the incorrectly identified system shown in Fig. 10(c) to improve training by using it as knowledge. We include plots of p_c against q_c for the incorrectly identified system and the trained neural network. As expected, the plot for the incorrectly identified system is bounded while the plot for the trained neural network is not, as shown in Fig. 11.

S6: Choosing Lookahead

While using $lookahead = 1$ works for any systems, a slightly larger lookahead may sometimes reduce the

training time. The choice of lookahead is based on both the choice of the training solver and system behaviors.

If the training solver incurs significant numerical errors at every step, the lookahead should be small. Large numerical error happens if the numerical integration scheme uses very large steps or is of low order. Since a larger lookahead means more numerical integration steps, the numerical errors can propagate through the trajectory and get amplified, rendering the resulting loss inaccurate.

Moreover, if the trajectory of a system is sensitive to slight perturbations to its initial conditions (e.g. the system has a positive Lyapunov exponent), the chosen lookahead should be close to 1. In this case, it's unreasonable to compare trajectories for long duration of time since the trajectories will diverge very quickly. In contrast, if a system is stable, the training should converge for any choice of lookaheads.

To further illustrate, a neural network is trained with the architecture in Table II on observations of the chaotic Lorenz attractor with different lookaheads. The training is stopped if the resulting trajectory gives $K_c \approx 1$ and the root mean squared error between the first 200 steps of the predicted trajectory and true trajectory is less than 2. The results are summarized in Table VI. It can be seen that using a lookahead of 2 reduces the number of epochs needed for training. The training did not converge for using $lookahead = 30$.

However, the time taken for training increases linearly with the lookahead since more numerical integration steps need to be performed. To address this shortcoming, the subproblems can be trained in batches to improve training speed. We have experimentally demonstrated the effectiveness of batched training with the KS equation example: the neural network was trained on the observations in batches and it was able to capture the spatiotemporal chaos. Note that the proportional increase in training time is not reflected in Table VI because the training duration has many overheads including performing the 0-1 test every few epochs.

Lookahead	# of Epochs	Duration
1	1950	1.00
2	1650	1.13
3	2500	3.10
4	3900	4.39
5	1350	1.86
6	3150	4.17
7	3000	4.28
30	>5000	NA

Table VI: Training a neural network on the observations of the chaotic Lorenz attractor with Adam and a learning rate of 0.01 without batching. Duration is not the actual time taken for training, but the ratio with respect to the training time of using $lookahead = 1$.